Research Journal of Applied Sciences, Engineering and Technology 7(23): 4945-4965, 2014
DOI:10.19026/rjaset.7.887
ISSN: 2040-7459; e-ISSN: 2040-7467

Submitted: January 04, 2014 Accepted: February 25, 2014 Published: June 20, 2014

Research Article

Study on the Temperature Distribution of High Pour Point Oil by Integrated Method Based on Well Log, Geological Data and Experiment

[1]Yu Peng, [2]Tang Zhonghua, [2]Akhtar Malik Muhammad and [3]Muhsan Ehsan
[1]Faculty of Earth Resources, China University of Geosciences,
[2]School of Environmental Studies, China University of Geosciences, Wuhan 388 Lumo Lu, Wuhan 430074, Hubei Province, China
[3]Institute of Geophysics and Geomatics (IGG), China University of Geosciences, Wuhan, China

Abstract: High pour point oil reservoir contains various typical properties; such as a kind of high freezing point, high paraffin content and high cloud point temperature reservoir, while the temperature is regarded as high sensitive parameter for oil reservoirs. The current research aim is to develop and assess the effect by cold water flooding, the structure and properties model was built with the combination method of reservoir geological modeling and simulation. Various degrees of cold damage have deep relation with paraffin deposition and reservoir channel plug due to decline of temperature below the cloud point temperature. Precipitated paraffin has changed the rheological properties of crude oil, which can increase filtration resistance and reducing the oil displacement efficiency. Furthermore, model simulation analysis results compared under two different conditions cold and hot water flooding and predicted the inter well temperature field distribution belongs to reservoir through the model numerical simulation. Present study depicts that the integrated method base on log, geological data and experiment can predict and analysis the temperature variation efficiently, while thermal displacement method has efficiently improved the high pour-point oil reservoir development effect, increasing oil mobility and enhancing oil recovery.

Keywords: Cloud point temperature, cold damage, high pour point oil, numerical simulation, temperature field

INTRODUCTION

High pour point oil reservoirs are usually part of the developed oilfields in various regions worldwide. The oil present in form of light crude and currently, the development pattern is generally established by injected cold water. Cold water damage is a consequence of paraffin deposition from decline of temperature at production and injection wells due to gas expansion and evolution (Ring *et al*., 1994) or cold water injection eventually causing low sweep and rapid water encroachment (Bedrikovetsky, 1997; Leontaritis, 2005, 1996). Therefore, it is important to establish a solution of such reservoirs to get crude oil.

Cyclic steam stimulation is well known and most popular thermal oil recovery method used for heavy oil reservoirs. When the steam and heat rise then due to gravity mobilized oil move downward direction (Butler, 1991). The decreasing the wax appearance temperature, crude oil ceases to flow and is called pour point and the production, storage and transportation of this crude oil stop (Mishra *et al*., 1995; Khan *et al*., 2008; Mahto, 2010). The steam flooding approach is applied to enhance oil recovery after water flooding. Steam flooding is injected into light-oil low-permeability sand light-oil reservoir and enhances its oil recovery (Qiaoyun *et al*., 2013). Temperature is sensitive parameter because mechanical properties of rock depend on temperature. Stiffness and strength of rock have an inverse relationship with temperature (Lempp and Welte, 1994). The experimental results show that by adding small concentration of polymeric additive the viscosity of waxy oil decrease (Vikas, 2013). To solve wax deposition and pour point concerns issues use chemical injection method (Santosh, 2012).

To evaluate the particular oil reservoir properties, such as high pour point oil, many scholars, at home or abroad, have carried out a series of thermodynamic studies using hot water flooding, steam flooding and so on, are necessary for safe investment. Present experiments and field tests are in the majority, temperature simulation analysis which was specifically aimed at high pour point oil occupies little. Jingguan2 Block being on production for about 30 years and also a relatively matured cold water flooded reservoir, the flooding effective is always been not good. Forecasting analysis is known to predict the temperature distribution of inter-well which is the basis of development adjustment and this problem can only be solved by numerical simulation method. In cases of this

Corresponding Author: Yu Peng, Faculty of Earth Resources, China University of Geosciences, Wuhan 430074, China, Tel./Fax: 0086-13986096629/027-87436235

study modeling and numerical simulation integration method for the effective displacement at different temperatures base on log, geological data and experiment was applied by the relevant software; during modelling the best injection temperature was establish which may provide some guidance for future oil exploitation and adjusting of oilfield.

Local geological setting: Jingguan2 Block is located in Liaohe basin in the Jinganbao oil-bearing structure belt of Damintun depression North-East China in Xinmin city, Liaoning Province. The block is an anticline faulted structure with oil-bearing strata dipping in the southwest direction with major axis 2.8 km and minor axis 0.8 km within an area of 2.2 km^2. Base on the fault system of the block is subdivided into four major sealing faults. S_3^2-S_3^4 segment, the oil-bearing target zone is of the Shahejie formation of the Paleogene period (Eocene). The oil-bearing targeted zone distance below surface is approximately within the range 1000-2800 m with average porosity of 20.9% and permeability of 0.527 μm^2 of the area. The reservoir depositional environment belongs to the alluvial fan and fan delta depositional system with relatively fine sand body and complex depositional structure. Deposition is marked by lake water plane rise-decline process. Most of the sub-layers are heterogeneous with high reservoir zone thickness variation and poor horizontal connectivity (Fig. 1).

Cured oil production has a correlation with to apply high injection pressure having low injection efficiency and the reservoir pressure is low being slightly higher than saturation pressure and is characterized by insufficient natural energy. The reservoir has no gas cap, while the water at the edge and bottom is not affecting the reservoir. However due to sound reservoir description analysis oil development can be enhanced (Fig. 2).

Fig. 1: Study area with regional location

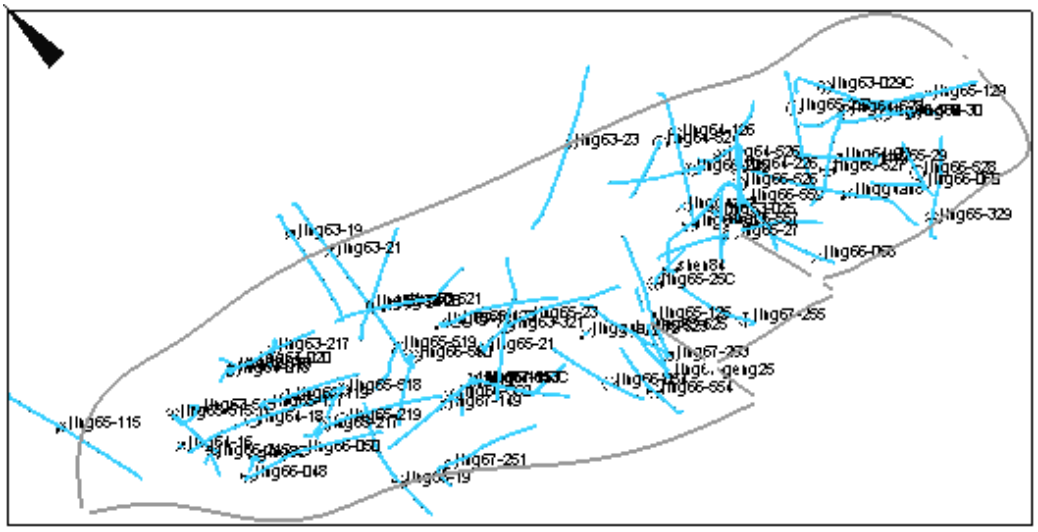

Fig. 2: Fault layout and well location distribution in Jingguan 2 block

METHODOLOGY

We use the method which based on log, geological data and experiment, first, we construct the geo-modeling based on the log and geological data, in this process and we first base the fault system data to construct the structure modeling. Depositional facies modeling was done using Petrel's interactive facies modeling tool based on existing sedimentary micro-facies map. Then, we use the linear regression method on wells core data and empirical formula to find the relation of Φ, K, Sw and log data's. We used Sequential Gaussian Simulation algorithm to generate the porosity model then we finish the modeling of object block. Then, we put this model be a basic model, use the software of Schlumberger's Eclipse to simulate the Jingguan 2 Block 30 years' water flooding situation, in this simulation process, we use thermal simulator to simulate that when injection temperature on different temperature situation, FrontSim was applied for simulation study with production data, the variation of distribution of temperature field of every sub-layer and distribution of remaining oil of every sub-layer.

RESULTS AND DISCUSSION

The model development on the reservoir: The reservoir model was developed base on acquired local well logs interpretation and prior zonation of the reservoir from which the reservoir structure was built. The reservoir was zoned into twelve different zones containing 93 sub-layers (Sub-layerII nomenclature) as seen below (Table 1). Sub-layerI nomenclature was adopted based on data availability as "effective oil thickness" here in referred to as Net-Pay base on the nomenclature Sub-layerI, while formation thickness referred to as Well Top in "Petrel" and depositional facies system were based on nomenclature Sub-layerII. Net Pay, depositional facies and faults were utilized by digitizing the prior available maps on Jingguan2 Block. The fault structure was digitized in Surfer based on the reservoir top surface map, S_3^2 top surface map, S_3^3 top surface map and S_3^4 top surface map to enable and accommodate the inclination of the faults in 3D. Fault polygons generated which are the backbone for the creation of the fault model (Fig. 3a) of the reservoir model while the WellTop generated the reservoir

Table 1: Reservoir zonation and sub-layer nomenclature adopted (unit of layer)

		Zone				Sub-layer I			Sub-layer II			Monolayer		
Formation	Sub-member	Identifier	Thickness /m	Sequence boundary	Sequence stratigraphy	Number		Identifier	Number		Identifier	Number		Identifier
S_3	S_3^1		0-285	SB5	SQ5	Not divided into oil layer group								
	S_3^2	I	50-70	F4	SQ4	3	13	1-3	6	28	1-6	Not divided into monolayer		
		II	50-69			3		1-3	6		1-6			
		III	82-99			4		1-4	10		1-10			
		IV	59-72	SB4		3		1-3	6		1-6			
	S_3^3	0	48-62	F3	SQ3	2	13	1-2	4	30	1-4	9	64	1-9
		I	113-129			4		1-4	9		1-9	19		1-19
		II	97-119			3		1-3	8		1-8	17		1-17
		III	127-152	SB3		4		1-4	9		1-9	19		1-19
	S_3^4	I	78-95	F2	SQ2	3	14	1-3	6	35	1-6	16	33	1-16
		II	73-94	SB2		4		1-4	8		1-8	17		1-17
		III	89-113			3		1-3	8		1-8	Not divided into monolayer		
		IV	146-171	SB1 (F1)	SQ1	4		1-4	13		1-13			
Total						40			93		97			

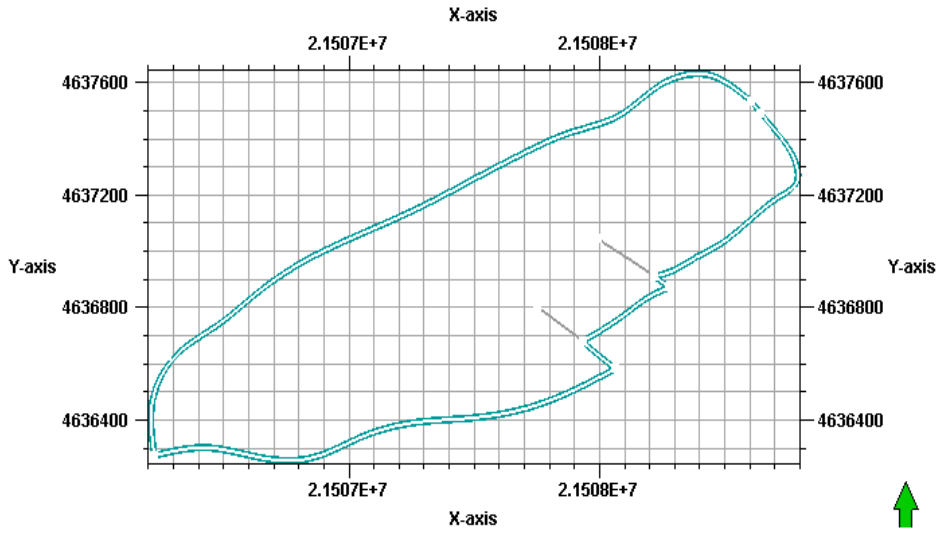

(a)

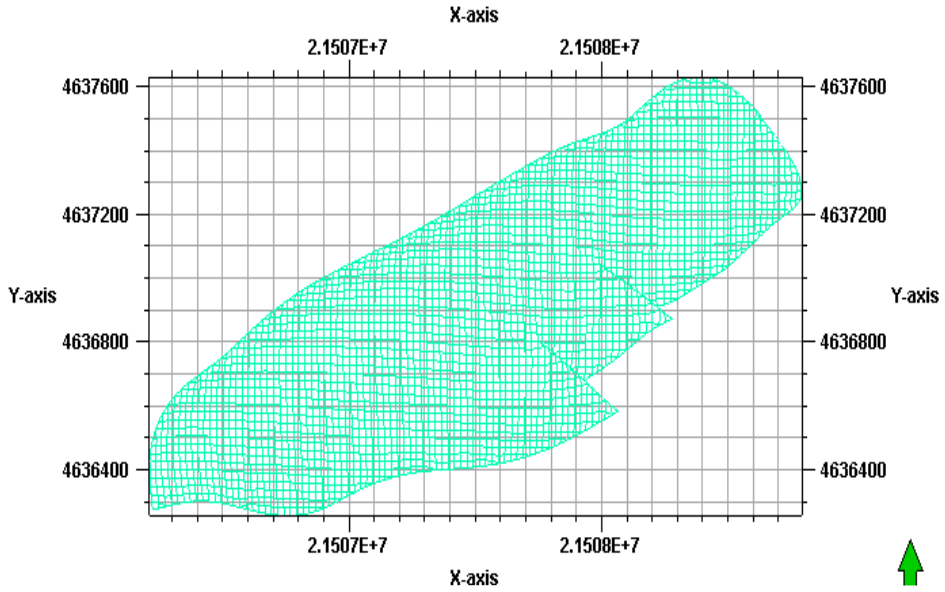

(b)

Fig. 3: 2D distribution map of fine grid model in Jingguan 2 block, (a) fault boundary, (b) 2D grid system

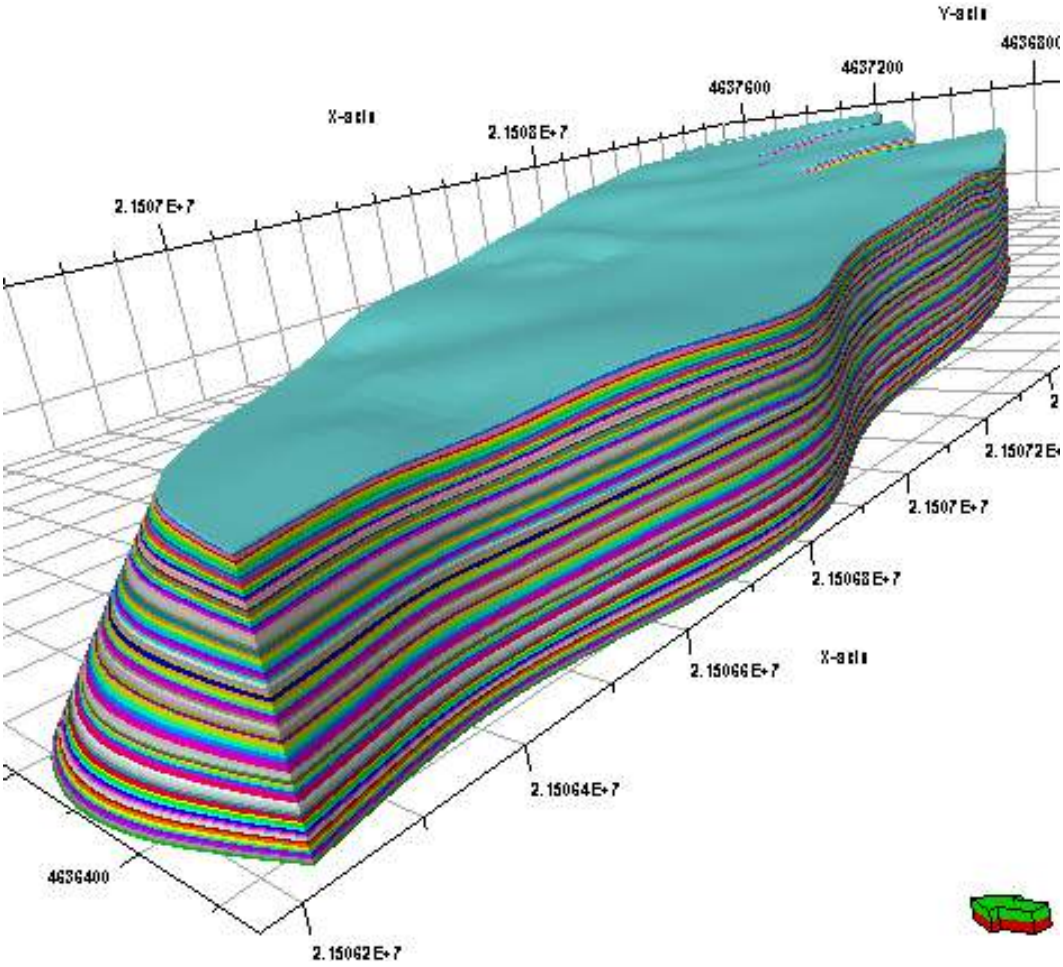

(a)

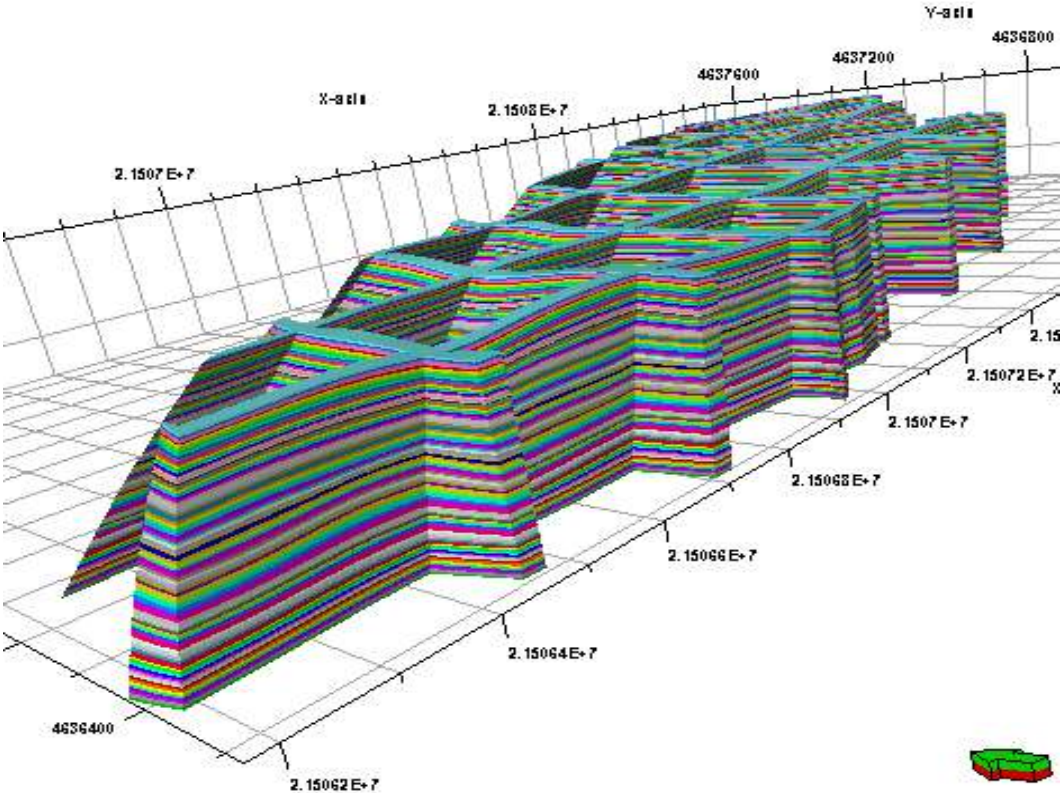
Y-axis
4636800
4637200
4637600
X-axis
2.1508E+7
2.1507E+7
2.15072E+7
2.1507E+7
2.15068E+7
2.15066E+7
2.15064E+7
4636400
2.15062E+7

(b)

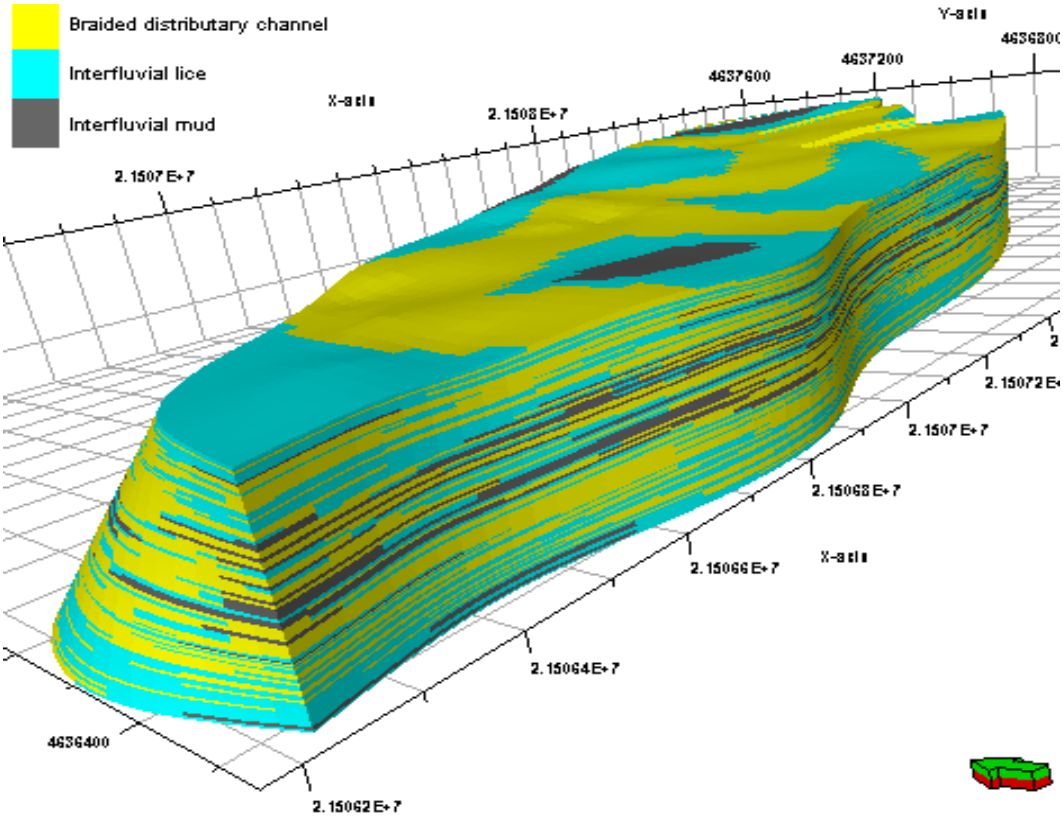
Braided distributary channel
Interfluvial lice
Interfluvial mud
Y-axis
4636800
4637200
4637600
X-axis
2.1508E+7
2.1507E+7
2.15072E+
2.1507E+7
2.15068E+7
2.15066E+7
X-axis
2.15064E+7
4636400
2.15062E+7

(c)

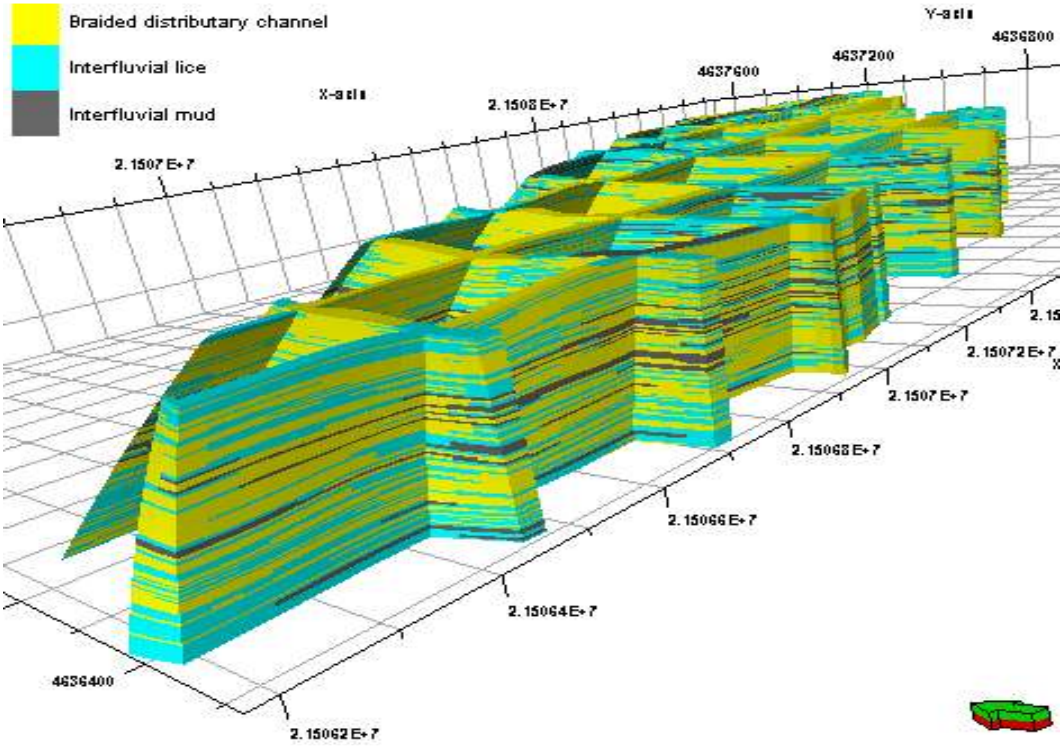

(d)

Fig. 4: Zones and facies models of Jingguan 2 block, (a) sub-layers model, (b) sub-layers fence diagram, (c) sub-layers grouped depositional facies model, (d) sub-layers grouped depositional facies fence diagram

structure in combination with the fault model. The initial 2D grid system was built based on the faults and the reservoir boundary polygon generated from digitizing Jingguan 2 Block surface to cover all the wells visible on the map and contained in the reservoir area and zone under study (Fig. 3b). Grid orientation was based on the major sealing fault that was located in the southwest. (3D) grid system construction was developed base on horizons and zones from Well top to establish the final reservoir 3D structure model. No further layering was established so as to retain the existing zonation of sub-layers for property modeling (Fig. 4a, b). The grid model was not up scaled prior to exporting to the fluid simulator after incorporating the various rock and fluid properties as the system was not considered a very fine gird or coarse grid.

Jingguan2 heterogeneity can be observed from the geological model of the group depositional facies which contains about 3 depositional facies comprising of braided distributary channel, interfluvial lice and interfluvial mud (Fig. 4c). And sand distribution direction is NE-SW. The sub-layers grouped depositional facies fence diagram symbolized the bad vertical connectivity of sand bodies (Fig. 4d). Depositional facies modeling was modeled using Petrel's interactive facies modeling tool based on existing sedimentary microfacies map. The essence of the facies model was to enable conditioning of porosity modeling in terms of trends with the depositional environment.

Evaluation petro physical characterization through modeling: Through developing various models technique petro physical characteristics were evaluated. Base on available well logs data which enable to define the correlation among the reservoir characterization such as porosity, permeability and water saturation. A number of logs data are available and these wells are located and covered Jingguan 2 reservoirs. The main logs available are SP, AC, RT, RE, RXO, RLLD, RLLS, RL3D, RL3S, RD and RS, other relevant logs not in sufficient number are GR, RHOB, DEN and COND. Selection of wells for the developing of correlation was based on the availability of AC log and zone of coverage of the log for the wells extract for log-core analysis and derivation of petrophysical property (Ambastha and Moynihan, 1996; Kamel and Mohamed, 2006). Each model methodology and description is presented one by one in detail.

Porosity analysis model: Correlation was set for the prior established zones based on linear regression to establish the relationship in Eq. (1) (Wyllie *et al*., 1958):

$$\Phi = a + m \cdot AC \quad (1)$$

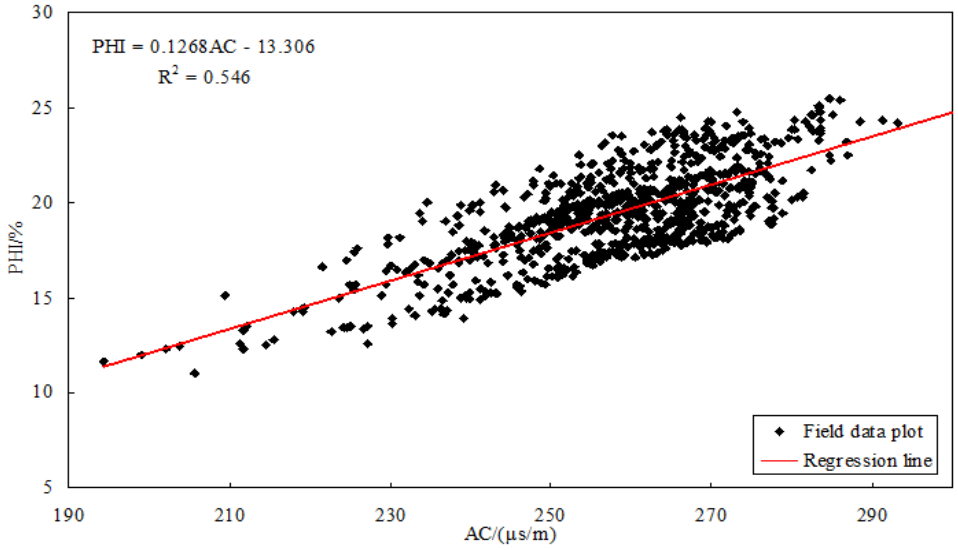

Fig. 5: PHI vs. AC correlation for filtered core porosity and acoustic log

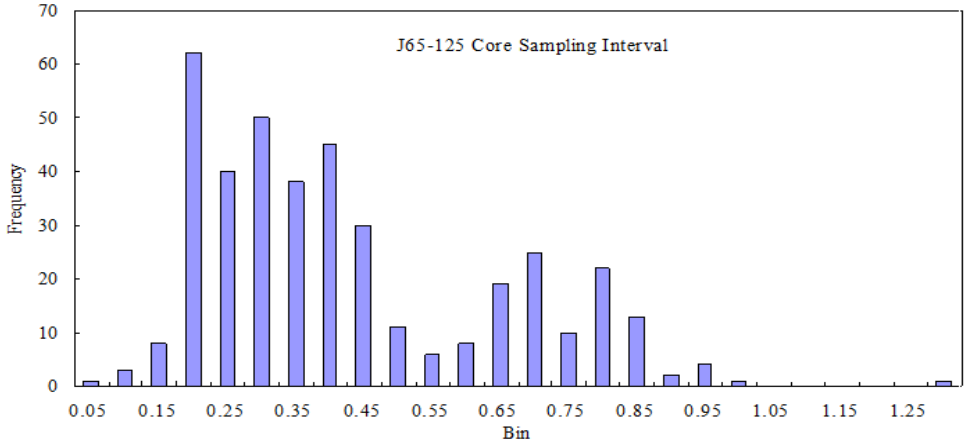

(a)

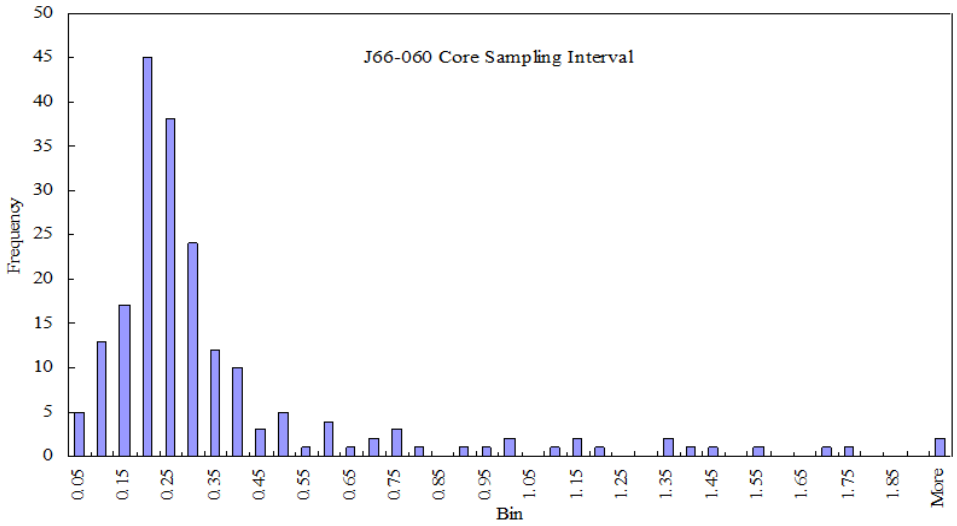

(b)

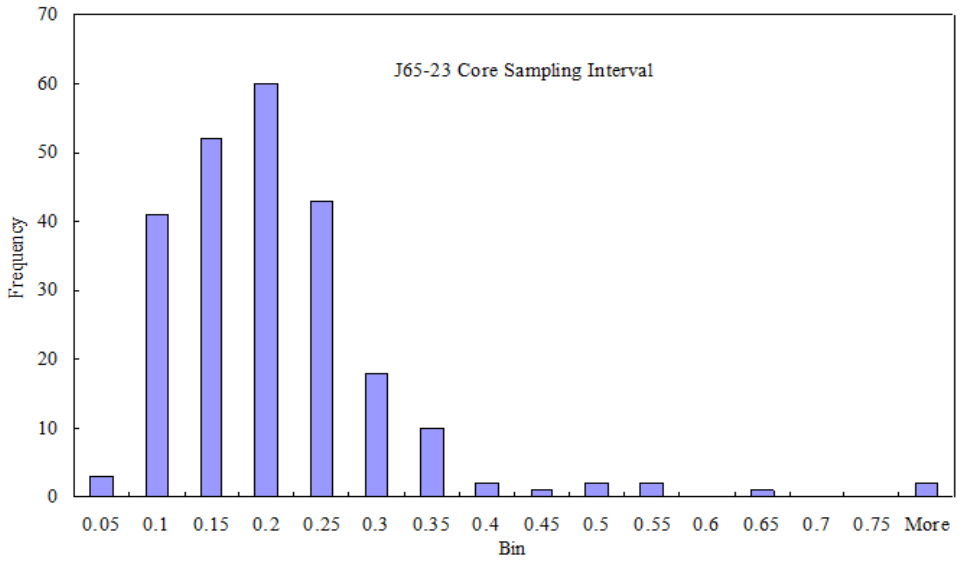

(c)

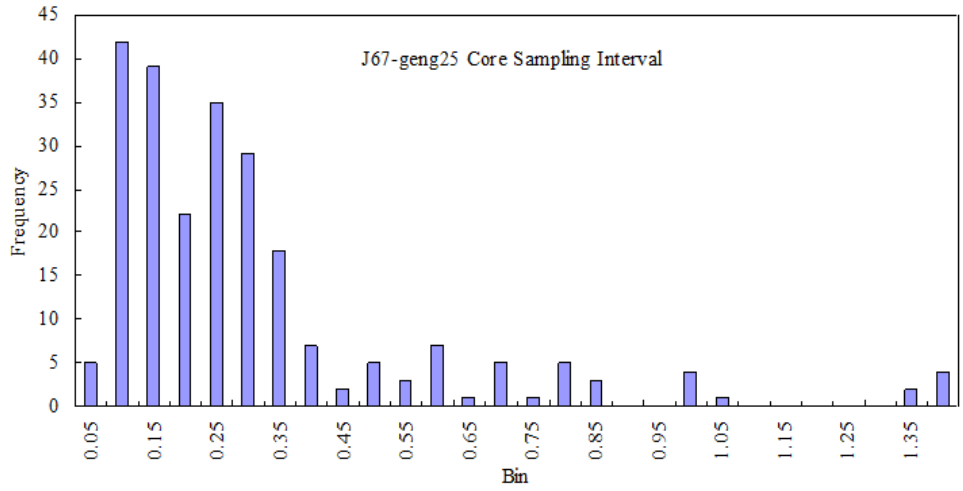

(d)

Fig. 6: Core sampling interval distribution for wells, (a) J65-125, (b) J66-060, (c) J65-23, (d) J67-geng25

where,

Φ : Total effective core porosity from laboratory analysis in percentage (%)

AC : Used for acoustic log (μs/m)

a and m : Lithology coefficients from least square regression (a = -13.3060, m = 0.1268)

The basic traditional correlation method of cross plot of core porosity and Acoustic (AC) log (Fig. 5) was adopted based on four selected wells (J66-060, J64-18, J63-217 and J66-530) core data as no reasonable correlation between AC and core porosity was achievable for core data from well JG1 after depth shifting with its limited data points. Well J8 was not within the depth of consideration however the addition of its data to the correlation obtained from the other 4 wells showed minimal change on coefficient of determination. J66-060 and J64-18 showed the best coefficient of determination obtained, probable related to these wells high production rate which may be due to high sand thickness compared to the other cored wells.

All cored values were filtered using a three points filter to correspond to the vertical resolution of the well logs (Al-Ali and Worthington, 2005). Filtering took into account the core data point sampling interval for the various cored wells as seen in the distribution of Fig. 6. The resulting relationships were obtained base on removal of outliers and applied to AC logs of 74 wells which are evenly distributed within the block to obtain porosity for uncored wells.

Porosity was obtained and upscaled within an arithmetic algorithm in Petrel prior to data analysis

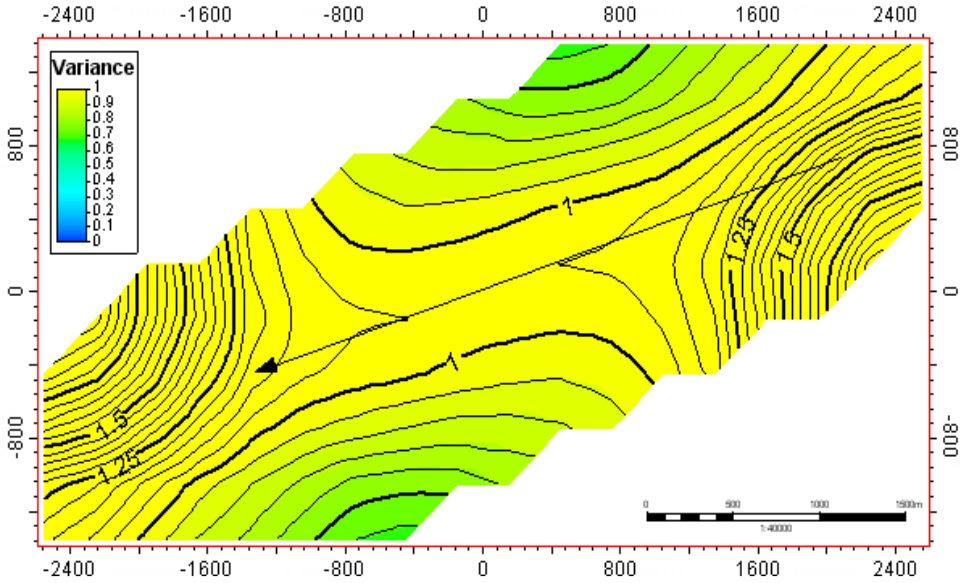

Fig. 7: Porosity variogram map to determine major and minor axis due to anisotropy for variogram analysis

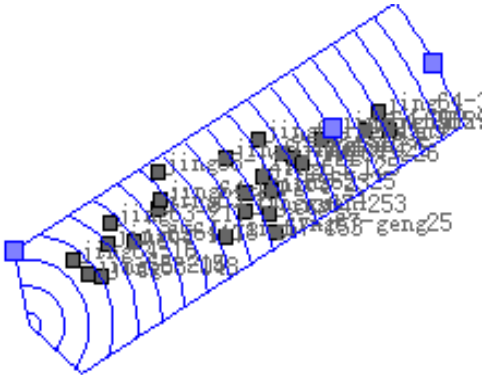

(a)

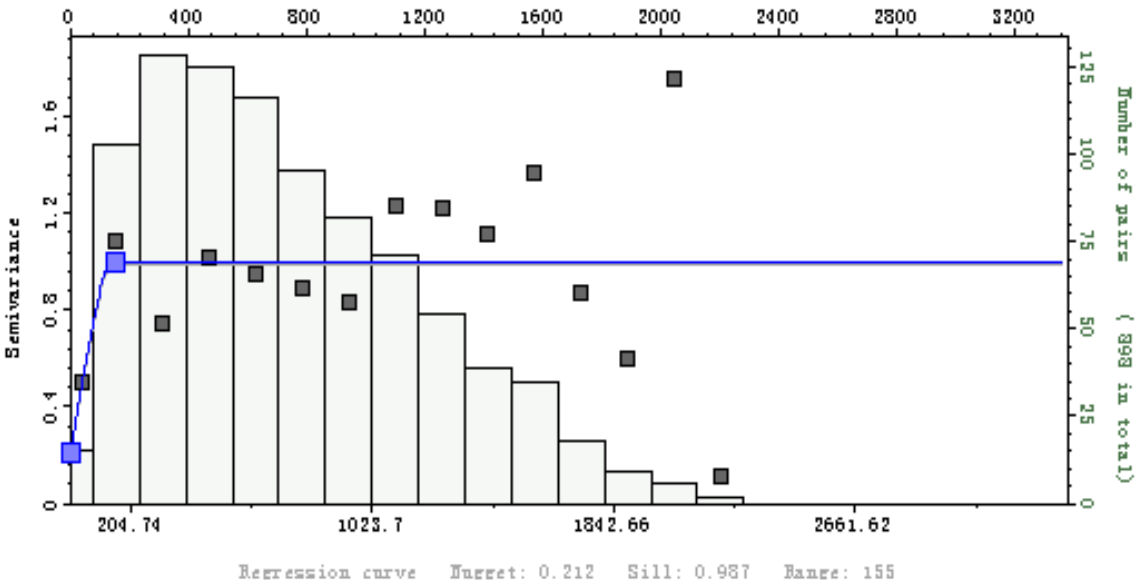

(b)

(c)

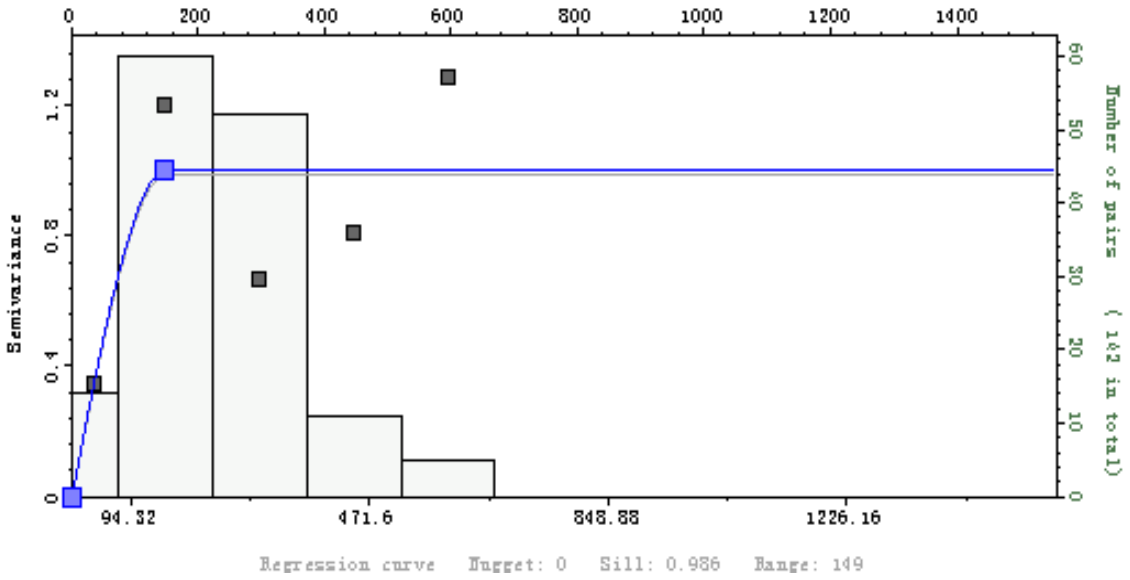

(d)

Fig. 8: Variograms analysis with porosity of S_3^3III4-9 in Jingguan 2 block, (a) major direction search cone: Tolerance: 71.6; Band: 430.4; Search: 3071.1; Lag: 157.5, (b) major direction semi-variance plot: Major: 155.4; Nugget: 0.212; Sill: 0.987, (c) minor direction search cone: Tolerance: 61.3; Band: 228.1; Search: 1414.8; Lag: 148.9, (d) major direction semi-variance plot: Major: 148.8; Nugget: 0; Sill: 0.986

conditioned by depositional facies to obtain the variogram (Fig. 7 and 8) and data transformation which has been used by Sequential Gaussian Simulation algorithm to generate the porosity model (Fig. 9). The model used for simulation and also presented in Fig. 8. It represents an arithmetic average of 10 stochastic realizations.

Permeability analysis model: Developed multi-variable regression of core porosity and well logs of AC, SP and RT depicted that there is a poor correlation as such core porosity and permeability linear regression was employed for analysis to establish the relation below for reservoir (Fig. 10):

$$K = a \cdot e^{b \cdot \Phi} \quad (2)$$

where,

k : Used for core laboratory analysis derived permeability (md)

Φ : Core derived total effective porosity (%)

a and b : Lithology related coefficient obtained from linear regression analysis (a = 0.0137, b = 0.3594)

However, AC and core porosity cross plot, porosity and permeability data showed a strong correlation among all factors (Corbett *et al*., 1998; Shahab *et al*., 1997). In present research, core data from the selected four wells (J66-060, J64-18, J63-217 and J66-530) were used for the analysis. The correlation so obtained was applied for all zones for calculating permeability based on log derived porosity from AC log of 74 wells that are evenly distributed in the block. Values obtained were upscaled with a geometric algorithm by the

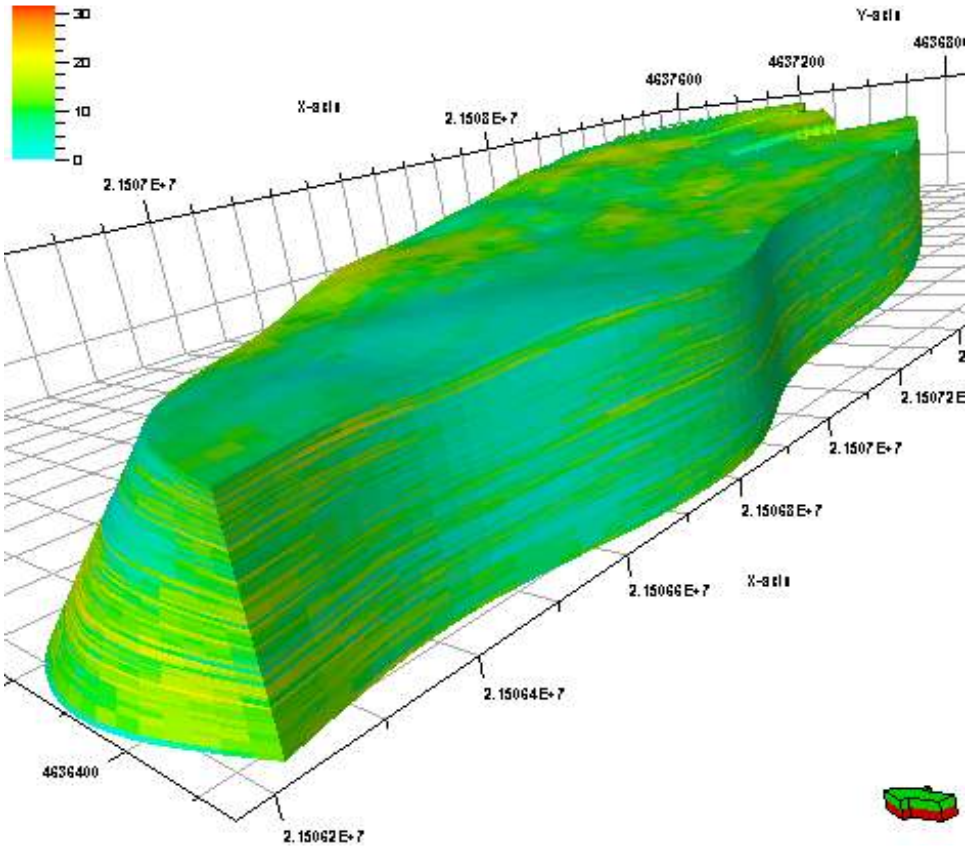

(a)

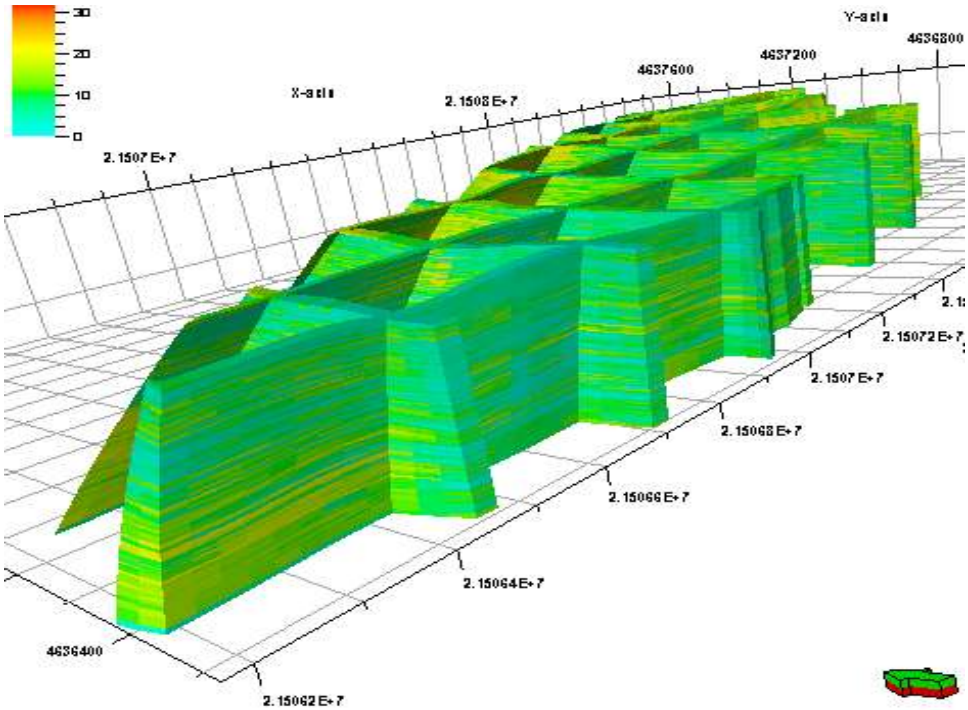

(b)

Fig. 9: Porosity model of Jingguan 2 block, (a) 3D model, (b) porosity model viewed with index and value filter turned on

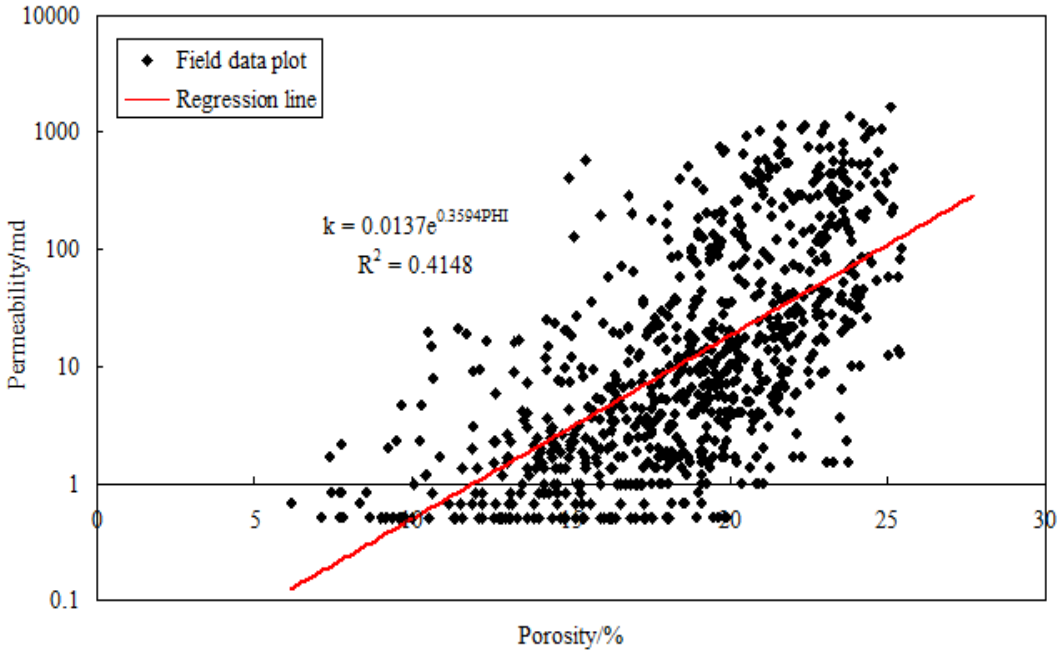

Fig. 10: Cross plot of core derived porosity and permeability for reservoir

modeling software prior to data analysis to derive variogram and carry out data transformation before Sequential Gaussian Simulation modeling that was conditioned to the porosity model being a secondary variable. The final permeability model (Fig. 11) is an average of 10 stochastic realizations to enhance the estimate of values.

Water saturation analysis model: Archie's equation (Archie, 1942) is widely used for estimating water saturation however the presence of shale undermines the accuracy of its use due to bound water inherent in shale. Though conductivity model is better off than resistivity model (including V_{sh} model), the availability of data confines the author to the use of resistivity model (McCoy and Grieves, 1997). The initial estimation of constant inputted data into Poupon-Leveaux (Indonesia) resistivity model Eq. (3) (Weiss *et al*., 1999) was obtained from the Pickett cross plot (Fig. 11). Saturation from Archie's formula Eq. (4) was compared with that of Indonesia formula (Fig. 12) and the latter model was a better match necessitating its use. Water resistivity (R_w) and cementation factor (m) both came from the Pickett plot while the initial estimate of saturation exponent (n) was taken as 2.0 been a widely accepted for consolidated sandstone reservoir, but was altered for a better fit in the process of getting a better match. V_{sh} value came from SP Eq. (5) and was useful as 69 well logs had SP logs. Ideally, V_{sh} must be computed from the product of shale index (I_{sh}) and rock density/shale density ratio but the use of V_{sh} was confined to Eq. (5) for each well has a reasonable estimate. All developed SP logs from the wells which had only negative SP values where discarded and were not used for computing water saturation from the correlation equation derived by matching core determined saturation available for only one well (J67-geng25) (Fig. 13):

$$S_w = \left(\left[\frac{V_{sh}^{\,1-(V_{sh}/2)}}{\sqrt{R_{sh}}} + \frac{\phi^{m/2}}{\sqrt{a \times R_w}} \right]^2 R_t \right)^{-1/n} \quad (3)$$

where,

S_w = Used for water saturation (%)
V_{sh} = Shale volume (%)
Φ = Log derived porosity (%)
R_{sh} = Shale resistivity
R_w = Water resistivity (ohm-m)
R_t = Deep resistivity (ohm-m)
m = Cementation exponential
n = Saturation exponent and a an electrical parameter (one of Archie's constants)

Based on calibration, the values for the constants of Eq. (3) are a = 1; n = 2.2; m = 1.861 and R_{sh} = 2; however 0.5 was a better match but with a considerable number of lower estimates for S_w than that of 2.0; R_w = 0.0677:

$$S_w = \left[(aR_w) / (\phi^m R_t) \right]^{1/n} \quad (4)$$

$$V_{sh} = (SP - SP_{\min}) / (SP_{\max} - SP_{\min}) \quad (5)$$

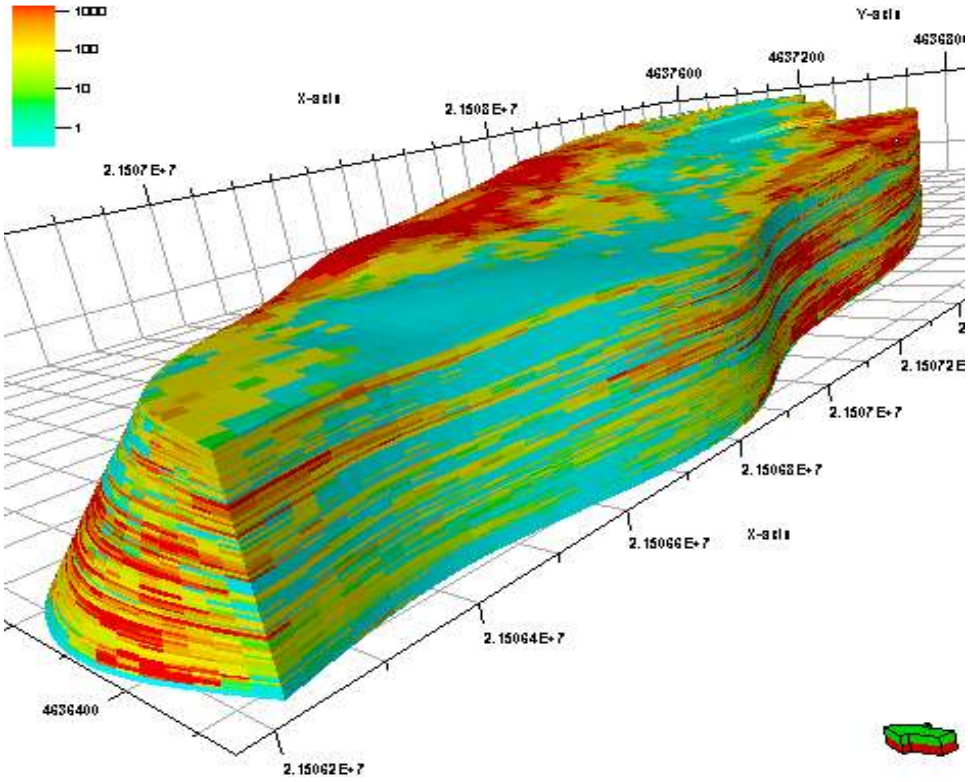

(a)

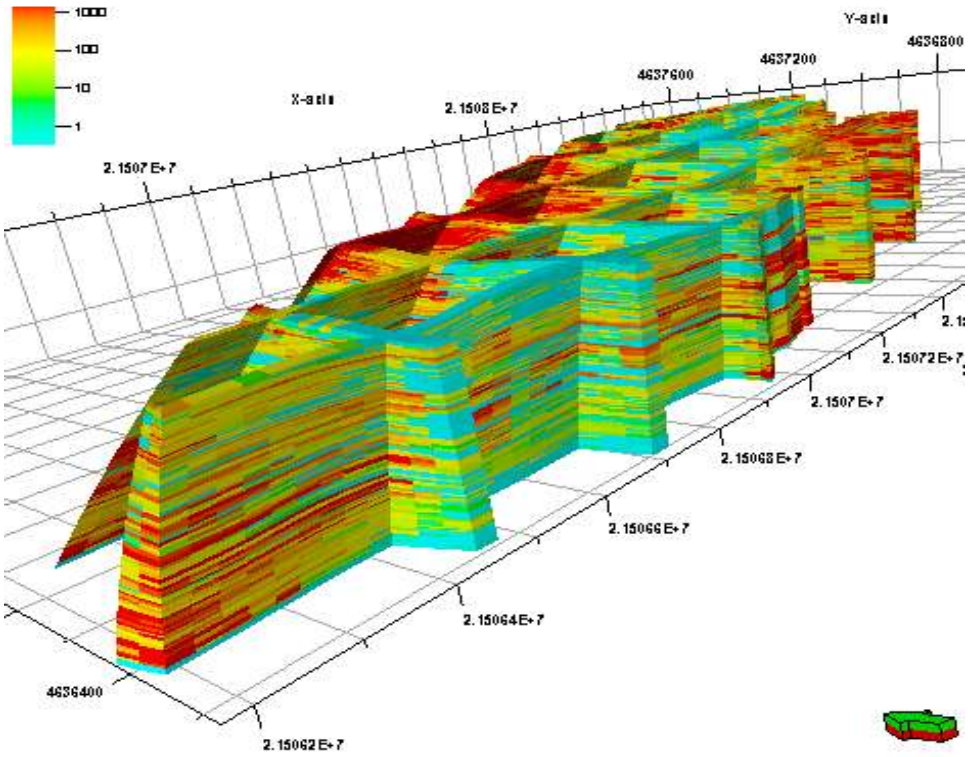

(b)

Fig. 11: Permeability model of Jingguan 2 block, (a) 3D model, (b) permeability model viewed with index and value filter turned on

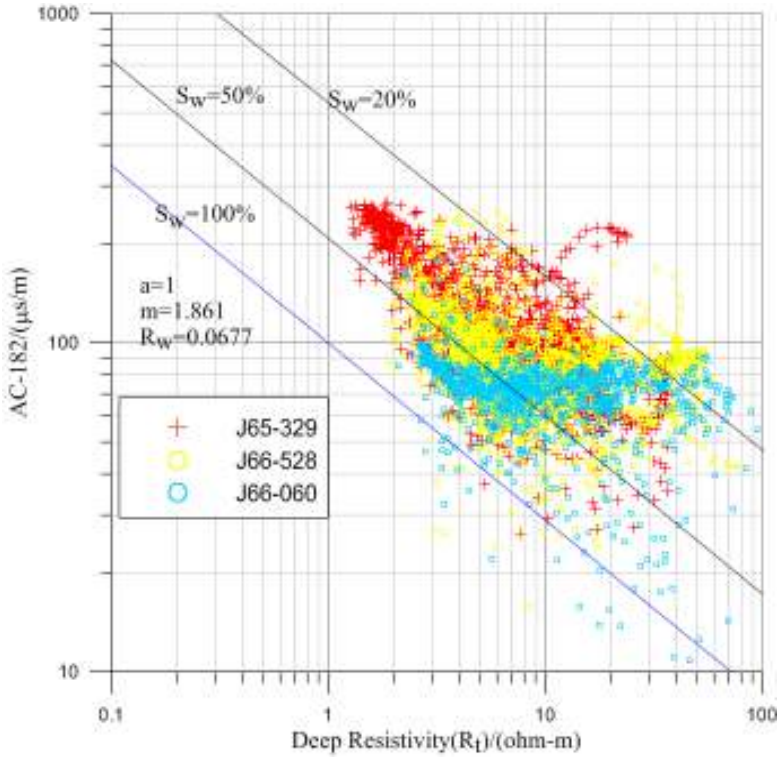

(a)

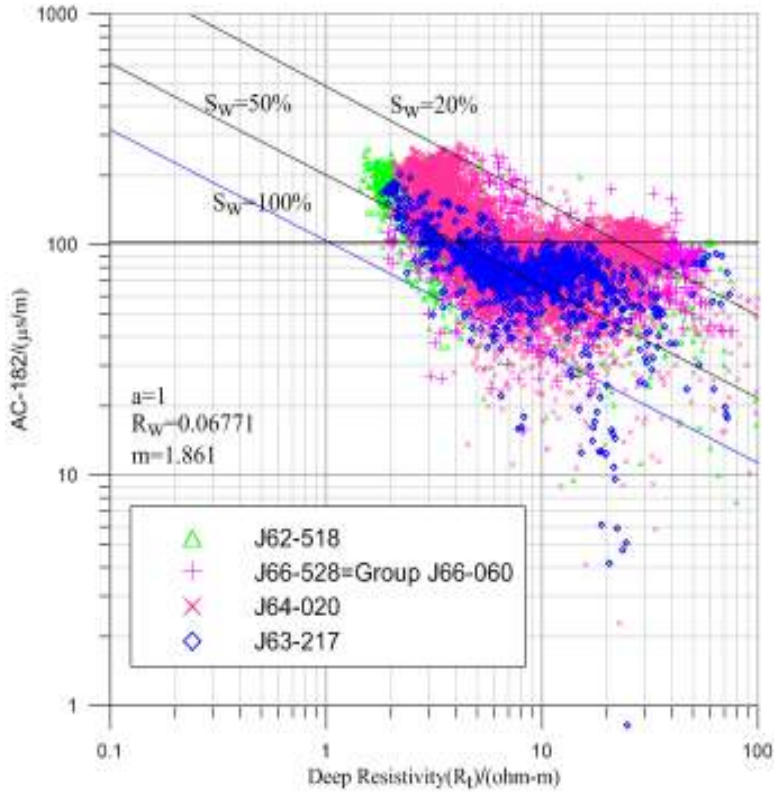

(b)

Fig. 12: Deep resistivity vs. AC cross plot, (a) pickett plot for group J66-060, (b) pickett plot for group J63-217

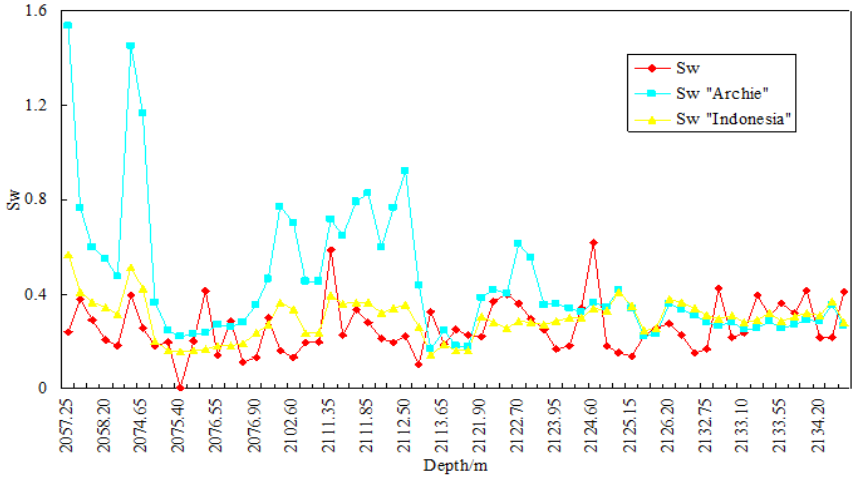

(a)

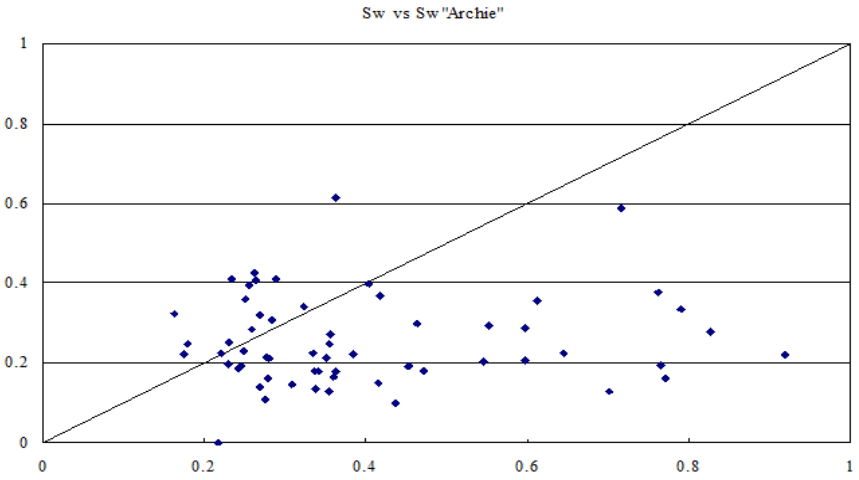

(b)

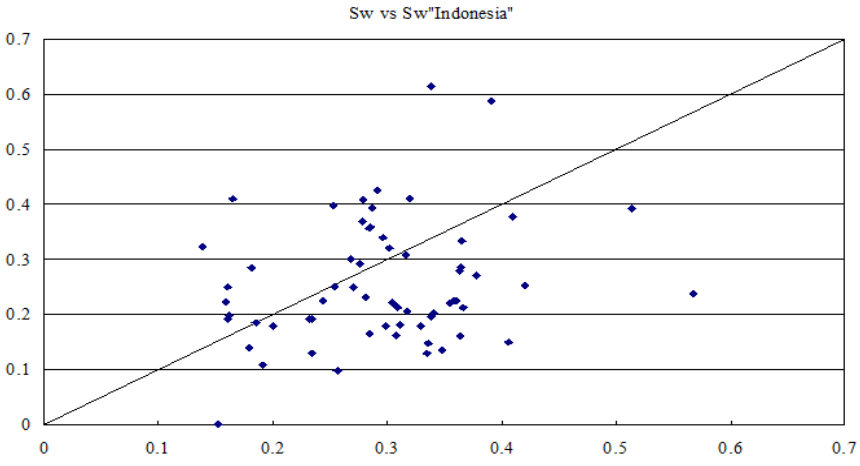

(c)

Fig. 13: Composite plot consisting of water saturation related plots, (a) water saturation calibration with well J67-geng25, (b) well J67-geng25 S_w core and archie computed, (c) well J67-geng25 S_w core and Indonesia computed

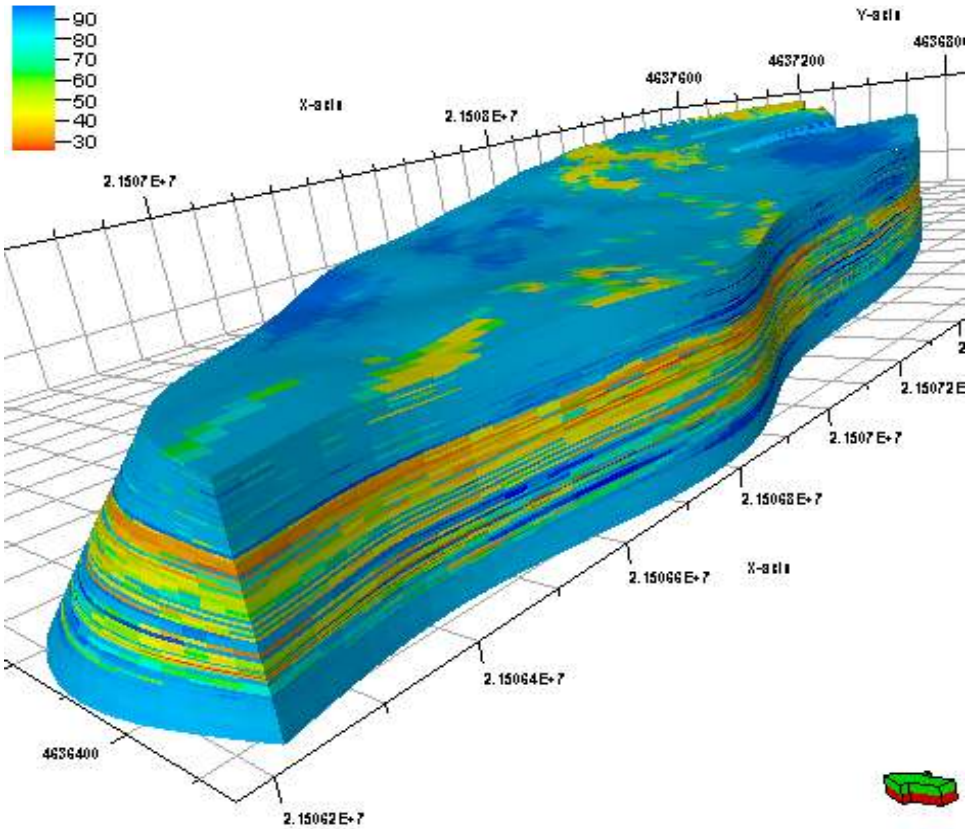

(a)

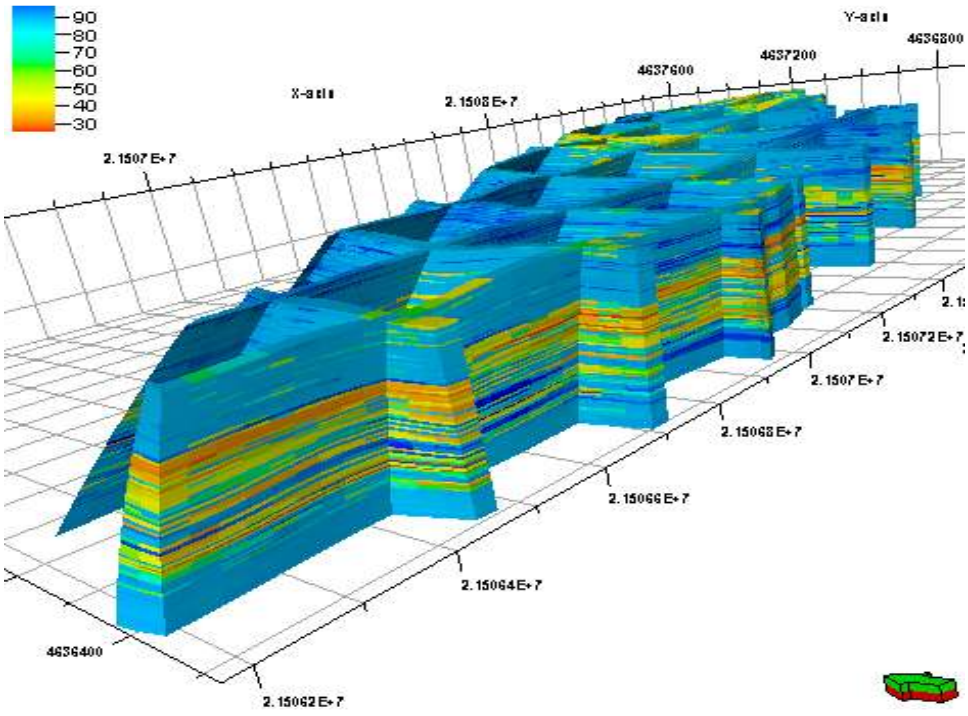

(b)

Fig. 14: Water saturation model of Jingguan 2 block, (a) 3D model, (b) water saturation model viewed with index and value filter turned on

The estimated correlation was used to compute water saturation value. Obtained values were upscaled with the help of an arithmetic algorithm through the modeling software prior to data analysis to develop variogram and data transformation before Sequential Gaussian Simulation modeling. The final saturation model is depicted in Fig. 14 and in an arithmetic average of 10 stochastic realizations to enhance estimated values.

THE THEORY AND THERMAL SIMULATIONS MODEL

Eclipse thermal simulator was used for simulation the study area through the produced data for 78 wells located in Jingguan 2 Block spanning a period of about 30 years. Aquifer support was not considered and the field is known to have insufficient natural energy and possess intercalated water layers. The 3D grid system was applied with the 104×55×93 cells in the direction of x, y and z, respectively. While the average value of Δx is 23.69, Δy is 23.21 and Δz values are varing, of which the representative cell flow equation is shown in Eq. (6) and (7) for multiphase flow without a dispersion term:

$$\sum_{j=1}^{N_p}\iiint_V \frac{\partial}{\partial T}(\varphi\rho_j\chi_{ij})dv + \sum_{j=1}^{N_p}\iint_S (\rho_j S_j \chi_{ij}\upsilon_j)ds + q_i = 0$$
$$i = 1,2,\cdots,N_c \quad (6)$$

where,
φ = Porosity
ρ_j = Density of phase j
S_j = Saturation of phase j
v_j = Surface flow velocity of phase j
x_{ij} = Mole fraction of component i
q_i = Source sink term of component i
N_p = Number of phases:

$$\iiint_V \frac{\partial}{\partial T}[\varphi\sum_{j=1}^{N_p}\rho_j S_j u_j + (1-\varphi)\rho_{rock}C_p(T-T_i)]dv + \iint_S (q_h + q_c)ds + Q_c + Q_h = 0 \quad (7)$$

where,
u_j = Internal energy of phase j
ρ_{rock} = Density of rock
C_p = Heat capacity at constant pressure
T_i = Initial temperature
q_h = Flow rate of enthalpy
q_c = Flow rate of heat
Q_c = Source of heat
Q_h = Source of enthalpy

Experimental analysis of the characteristics of high pour point oil: High pour point oil reservoirs have very complex geological mechanism because of its unique phase variation. In order to analyze the influence of water injection temperature changes on the percolation characteristics of high pour point crude, cores and sample of Jingguan 2 Block were used for an experimental study on oil flow ability as temperature change and its permeability and the full viscosity-temperature curves were simultaneously determined. The implementation of this experiment had two processes: First step was applied to increase and decrease temperature and the crude oil displacement experiment were to test the flow velocity at 40, 50 and 60°C, respectively.

Law of high pour point oil and relative permeability curve: The relative permeability of oil and water flow changes with the variation of temperature (Ramey Jr., 1962). High pour point oil has based with Newtonian fluid and the formation of higher temperature higher than cloud point and relative permeability curve can be measured by usual methods in this environment. Seepage law may be about to change when the temperature drops below that cloud point and the crude oil is non-Newtonian fluid in a porous medium (Huang *et al*., 2008). As the temperature rises, the irreducible water saturation increases and the residual oil saturation decreases based on laboratories studies. Relative permeability curve was tested under different temperatures seniors with respect to the collected data and applied for simulation (Fig. 15).

Viscosity-temperature characteristics of high pour point oil: Viscosity is regarded as a sensitive factor to evaluate temperature of high pour point oil. The crude oil is characterized by Newtonian property and change in its viscosity was slight when the oil temperature is higher than cloud point. The viscosity of crude oil increased significantly when the wax crystals were precipitated and its temperature was laid between cloud and critical point. At the temperature lower than critical point, the characteristics of crude oil were presented as more wax crystals were precipitated. By this time the viscosity of crude oil is rising fairly rapidly with temperature reduced (Gao *et al*., 2008). Fit a representative viscosity-temperature curve for application in thermal model (Fig. 16).

Comparative analysis of cold and hot water displacement: FrontSim was used to simulate the study area with help of produced data for 78 wells, which are located in Jingguan 2 Block and for the period of about 30 years. The block was started production in the year 1984 which contains 51 production wells and 27 injection wells and reservoir cold damage is a consequence of the development way of cold water injection. The simulation result shows that injected water streamline was scattered with narrow swept area and high remaining oil saturation which demonstrated the low displacement efficiency of the block.

The injected water temperature has direct relation with the displacement efficiency and economic benefits

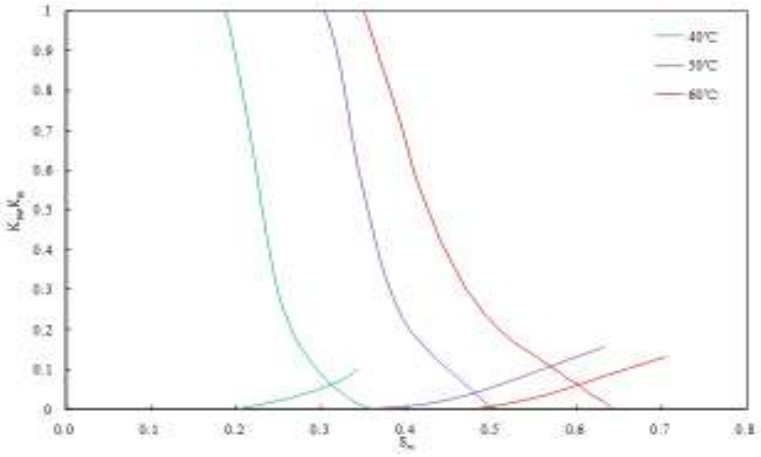

Fig. 15: Oil-water relative permeability curves at different temperatures

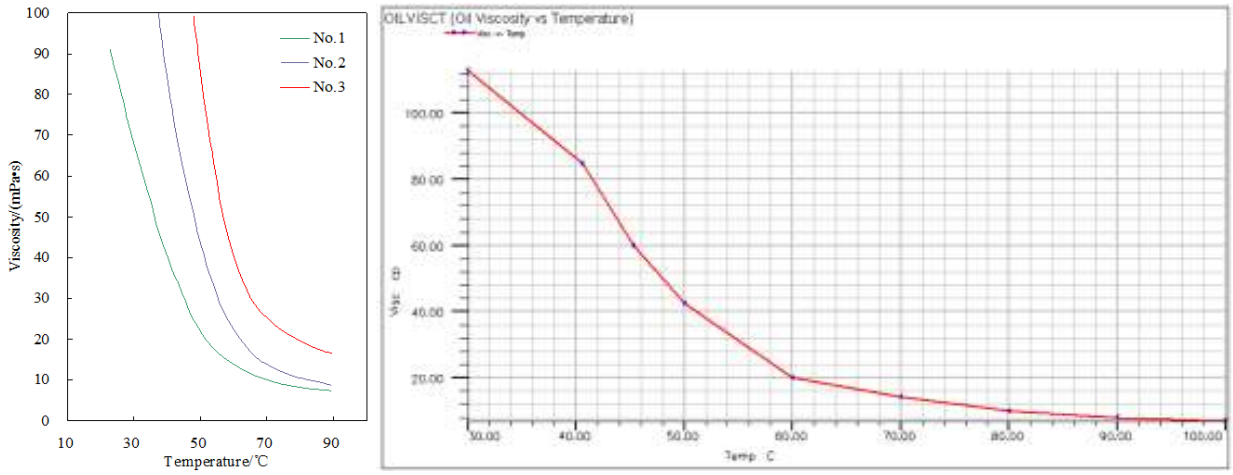

(a) (b)

Fig. 16: Viscosity and temperature curves of crude oil in Jingguan 2 block, (a) experimental data of well, (b) numerical simulation data

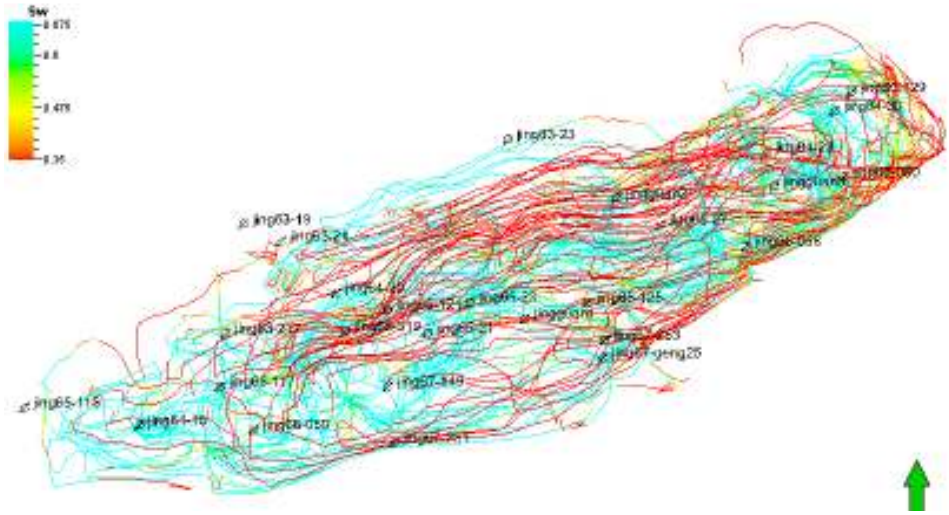

Fig. 17: Widespread of cold water flooding by frontsim in Jingguan 2 block (2013)

of the oilfield, simulating mining effects under different temperatures still have a guidance function to realistic development. The thermal method was used to simulate the law of oil-water movement under the cold and hot water injection condition. Figure 17 reflects the distribution of temperature field of sub-layer S_3^4- II-5 in Jingguan 2 Block in May 2000 when the frequency of water injection reached to its peak. In addition, a large area of low temperature in Fig. 18a shows that the temperature at the vicinity of water injection well is below the cloud point, the precipitated paraffin travels a short distance thereby making damage concentrated to reservoir. Hot water displacement can keep temperature on 65°C (Fig. 18b). Figure 10 shows that the hot water injection used leads to stronger formation water absorption and higher displacement efficiency. Distribution of temperature field of sub-layer S_3^4-II-5 in Jingguan 2 Block with hot water flooding in 2028

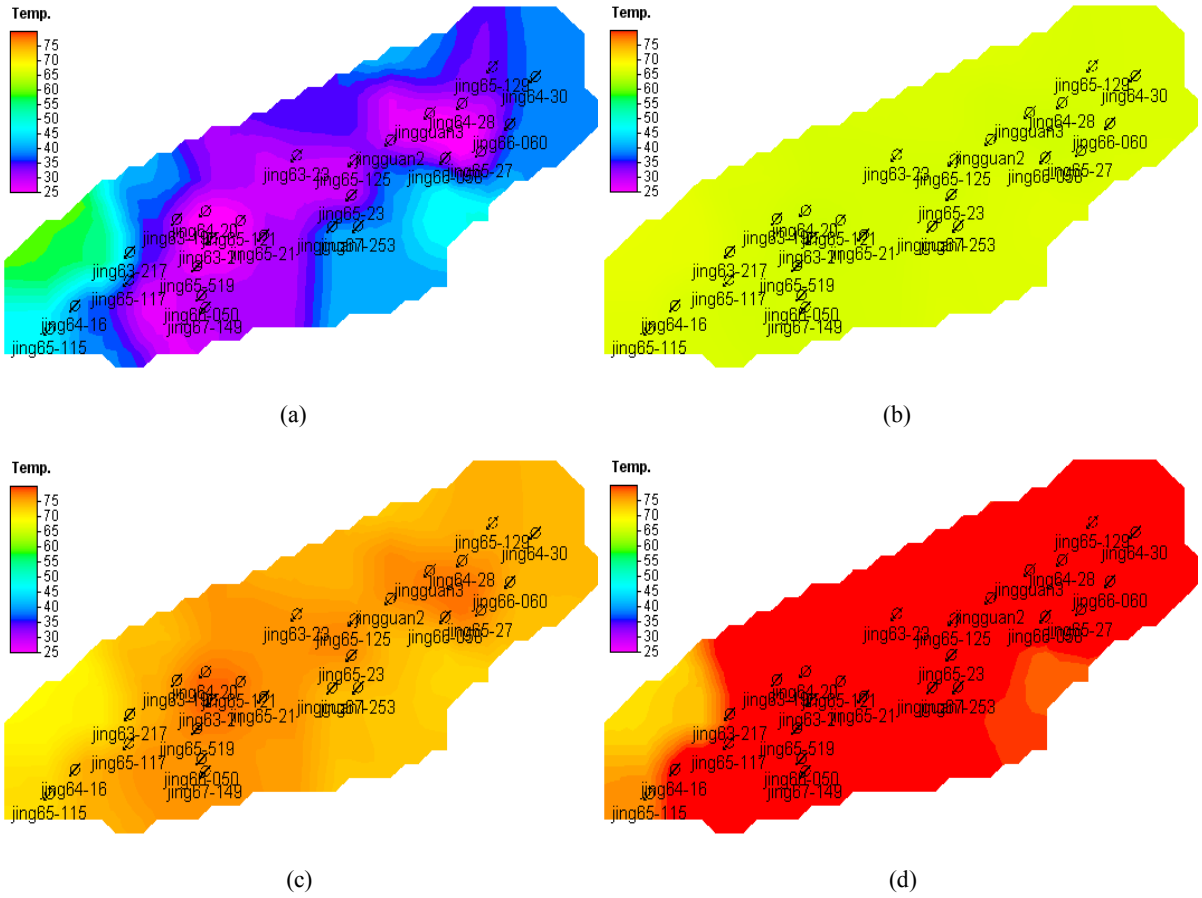

(a) (b)

(c) (d)

Fig. 18: Distribution of temperature field of sub-layer S_3^4-II-5 in Jingguan 2 block at different water injection temperatures (2000), (a) cold water flooding, (b) T_{winj} = 65°C, (c) T_{winj} = 80°C, (d) T_{winj} = 95°C

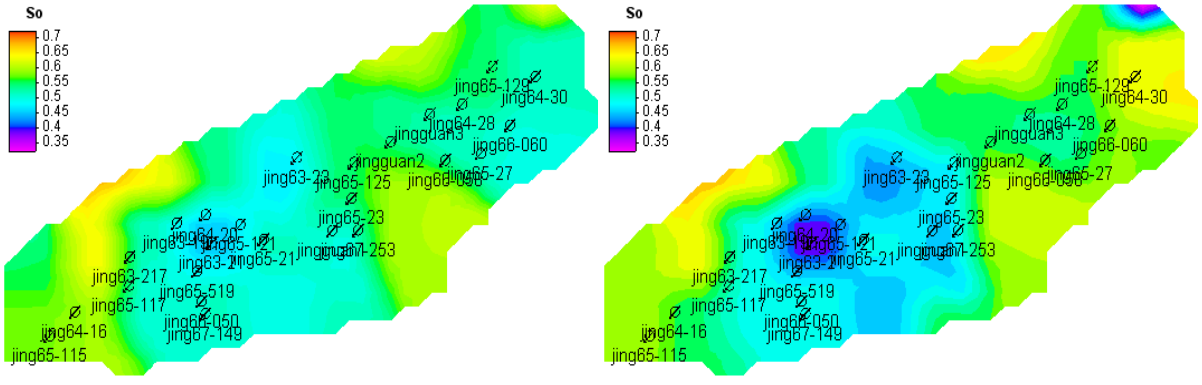

(a) (b)

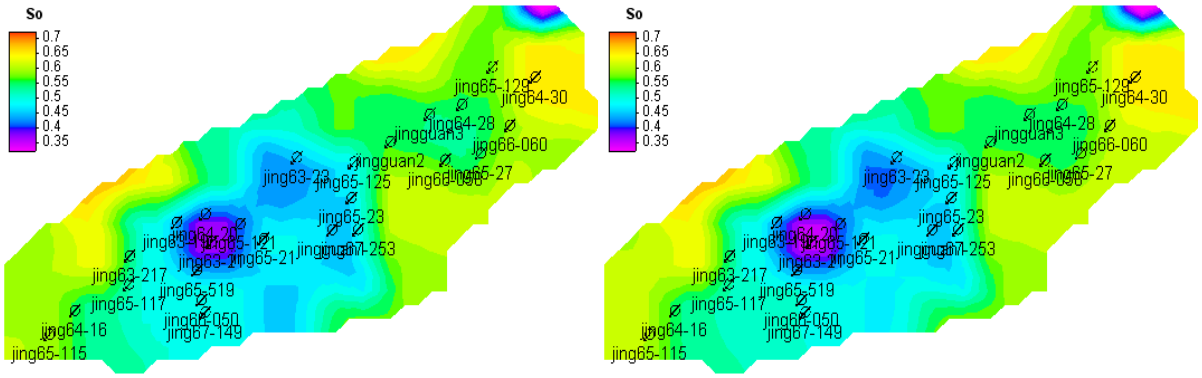

(c) (d)

Fig. 19: Distribution of remaining oil of sub-layer S_3^4-II-5 in Jingguan 2 block at different water injection temperatures (2000), (a) cold water flooding, (b) T_{winj} = 65°C, (c) T_{winj} = 80°C, (d) T_{winj} = 95°C

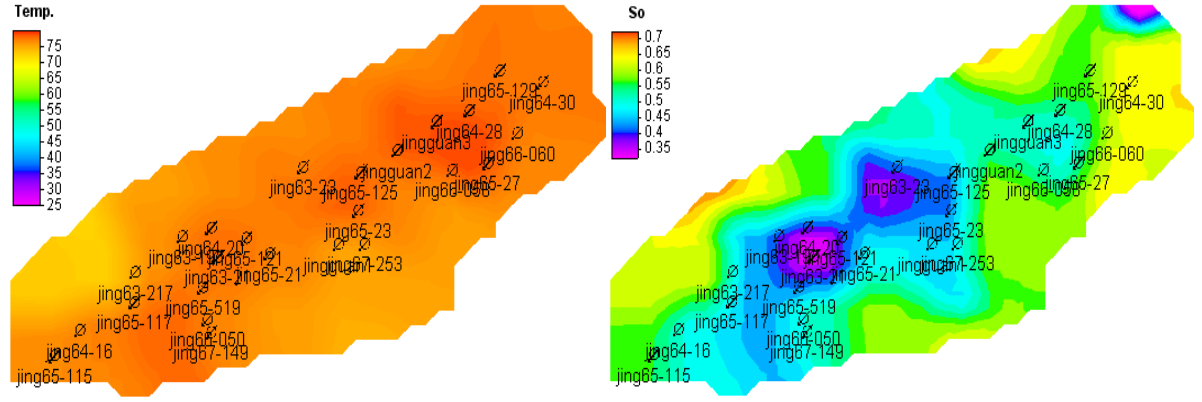

(a) (b)

Fig. 20: Distribution of temperature field and remaining oil of sub-layer S_3^4-II-5 in Jingguan 2 block with hot water flooding (2028) (T_{winj} = 80°C)

displays an excellent recovery efficiency which can keep reservoir temperature on the cloud point and also have the impact of reduce viscosity and enhance oil recovery (Fig. 19 and 20).

CONCLUSION

The followings are the main findings of the present study:

- J66-060 and J64-18 showed the best coefficient of determination obtained, probable related to these wells high production rate which may be due to high sand thickness compared to the other cored wells.
- The final permeability model (Fig. 10) is an average of 10 stochastic realizations to enhance the estimate of values.
- Saturation from Archie's formula Eq. (4) was compared with that of Indonesia formula (Fig. 12) and the latter model was a better match necessitating its use.
- The thermal simulation results indicate that thermal method can make reservoir temperature is higher than cloud point and increase the fluidity of crude oil.
- Temperature is a very sensitive parameter with oiling. Varying degrees of cold damage is a consequence of paraffin deposition and reservoir channel plug from decline of temperature below the cloud point temperature.
- Water injection temperature has greater influences on reservoir seepage law and recovery factor. Higher injection temperature can keep the reservoir temperature on cloud point, even makes that temperature increase, so as to improve the development effect. Higher injection temperature is not always better and the limit of development cost need to be considered. The water injection temperature 80°C was chosen for the optimal temperature.

REFERENCES

Al-Ali, H.A. and P.F. Worthington, 2005. Applications of petrophysical scale reconciliation to Saudi Arabian reservoirs. Proceeding of International Petroleum Technology Conference. Doha, Qatar.

Ambastha, A. and T. Moynihan, 1996. A simple and accurate method for an integrated analysis of core and log data to describe reservoir heterogeneity. J. Can. Petrol. Technol., 35(1): 8.

Archie, G.E., 1942. The electrical resistivity log as an aid in determining some reservoir characteristics. T. AIME, 146(99): 54-62.

Bedrikovetsky, P., 1997. Improved waterflooding in reservoirs of highly paraffinic oils. Proceeding of Latin American and Caribbean Petroleum Engineering Conference. Rio de Janeiro, Brazil.

Butler, R.M., 1991. Thermal Recovery of Oil and Bitumen. Prentice-Hall, Englewood Cliffs, NJ, pp: 285-359.

Corbett, P.W.M., J.L. Jensen and K.S. Sorbie, 1998. A review of up-scaling and cross-scaling issues in core and log data interpretation and prediction. Geol. Soc., London, Special Publications, 136(1): 9-16.

Gao, P., J.J. Zhang, L. Hou and H.F. Wang, 2008. Relationship between waxy crude viscosities and wax crystal microstructure. J. Cent. South Univ., T., 15: 406-410.

Huang, S.X., X. Chen, C.J. Lu, L. Hou and Y.R. Fan, 2008. Non-Newtonian steady shear flow characteristics of waxy crude oil. J. Cent. South Univ., T., 15: 326-328.

Kamel, M.H. and M.M. Mohamed, 2006. Effective porosity determination in clean/shaly formations from acoustic logs with applications. J. Petrol. Sci. Eng., 51(3): 267-274.

Khan, A.R., V. Mahto, S.A. Fazal and S. Laik, 2008. Studies of wax deposition onset in case of Indian crude oil. Petrol. Sci. Technol., 26(14): 1706-1715.

Lempp, Ch. and D.H. Welte, 1994. The effect of temperature on rock mechanical properties and fracture mechanisms in source rocks-experimental results. Proceeding of Rock Mechanics in Petroleum Engineering. Delft, Netherlands.

Leontaritis, K.J., 1996. The asphaltene and wax deposition envelopes. Fuel Sci. Techn. Int., 14(1-2): 13-39.

Leontaritis, K.J., 2005. Asphaltene near-well-bore formation damage modeling. J. Energ. Resour-ASME, 127(3): 191-200.

Mahto, V., 2010. Study the rheological properties of Indian waxy crude oil. Proceedings of National Seminar on Recent Advances in Chemical Engineering, G.I.E.T. Gunupur.

McCoy, D.D. and W.A. Grieves, 1997. Use of resistivity logs to calculate water saturation at Prudhoe Bay. SPE Reservoir Eng., 12(1): 45-51.

Mishra, S., S. Baruah and K. Singh, 1995. Paraffin deposition in crude oil production and transportation: A review. SPE Prod. Facil., February: 50-54.

Qiaoyun, L., H. Liu, W. Shuhong, Z. Zhang, Q. Yu, D. Shen and Z. Xin, 2013. A case study: Steamflooding to enhance recovery of a waterflooded light-oil reservoir. Proceeding of SPE Asia Pacific Oil and Gas Conference and Exhibition. Jakarta, Indonesia, October 22-24.

Ramey Jr., H.J., 1962. Wellbore heat transmission. SPE J. Petrol. Technol., 14(4): 427-435.

Ring, J.N., R.A. Wattenbarger, J. Keating and S. Peddibhotla, 1994. Simulation of paraffin deposition in reservoirs. SPE Prod. Facil., 9(1): 36-42.

Santosh, C., 2012. Drilling and completion technologies to meet challenges of waxy, high pour-point oil production. Proceeding of 9th Binnial International Conference and Exposition on Petroleum. Hyderabad.

Shahab, M., B. Bogdan and A. Samuel, 1997. Permeability determination from well log data. SPE Formation Eval., 12(3): 170-174.

Weiss, W., S. Wo, R. Balch, J. Roe, K. Fagrelius and R. Kendall, 1999. Integrating core porosity and SW measurements with log values. Proceeding of SPE Rocky Mountain Regional Meeting. Gillette, Wyoming.

Wyllie, M.R.J., A.R. Gregory and G.H.F. Gardner, 1958. An experimental investigation of factors affecting elastic wave velocities in porous media. Geophysics, 23(3): 459-493.